

# QuCLEAR: Clifford Extraction and Absorption for Significant Reduction in Quantum Circuit Size

Ji Liu

Argonne National Laboratory  
Lemont, USA  
ji.liu@anl.gov

Alvin Gonzales

Argonne National Laboratory  
Lemont, USA  
agonzales@anl.gov

Benchen Huang

University of Chicago  
Chicago, USA  
benchenh@uchicago.edu

Zain Hamid Saleem

Argonne National Laboratory  
Lemont, USA  
zsaleem@anl.gov

Paul Hovland

Argonne National Laboratory  
Lemont, USA  
hovland@mcs.anl.gov

**Abstract**—Quantum computing carries significant potential for addressing practical problems. However, currently available quantum devices suffer from noisy quantum gates, which degrade the fidelity of executed quantum circuits. Therefore, quantum circuit optimization is crucial for obtaining useful results. In this paper, we present QuCLEAR, a compilation framework designed to optimize quantum circuits. QuCLEAR significantly reduces both the two-qubit gate count and the circuit depth through two novel optimization steps. First, we introduce the concept of Clifford Extraction, which extracts Clifford subcircuits to the end of the circuit while optimizing the gates. Second, since Clifford circuits are classically simulatable, we propose Clifford Absorption, which efficiently processes the extracted Clifford subcircuits classically. We demonstrate our framework on quantum simulation circuits, which have wide-ranging applications in quantum chemistry simulation, many-body physics, and combinatorial optimization problems. Near-term algorithms such as VQE and QAOA also fall within this category. Experimental results across various benchmarks show that QuCLEAR achieves up to a 77.7% reduction in CNOT gate count and up to an 84.1% reduction in entangling depth compared to state-of-the-art methods.

## I. INTRODUCTION

Quantum circuit optimization [1]–[13] is important in both the Noisy-Intermediate-Scale-Quantum (NISQ) era and the fault-tolerant quantum computing era. Since quantum gates are noisy and the number of gates directly impacts circuit execution time, optimizing these circuits is essential. Given that operations on quantum devices have higher error rates than those on classical devices, we must ask: “Do we need to run the entire circuit on quantum devices?” Hybrid algorithms such as VQE [14] and QAOA [15] demonstrate that the evaluation of unitaries can be combined with classical optimizers on classical devices. In this paper, we show that quantum circuit size can be further reduced with circuit optimization and classical post-processing. We demonstrate the effectiveness of this approach on quantum simulation circuits.

Quantum simulation (also known as Hamiltonian simulation) is an important class of quantum algorithms. Given a Hamiltonian  $H$  and evolution time  $t$ , the circuit imple-

ments the operator  $U = e^{-i\hat{H}t}$ . The operator is typically decomposed into the sum of local Hamiltonians [16] with trotterization [17] and the unitary is expressed in terms of a sequence of Pauli strings:  $U = e^{-iP_1t_1}e^{-iP_2t_2}\dots e^{-iP_k t_k}$ . In fact, any quantum circuit can be described through quantum simulation, as any unitary operation can be expressed in this form. Quantum simulation has numerous applications, including quantum chemistry [18], many-body physics [19], [20], and solving combinatorial optimization problems [21]. For near-term algorithms such as VQE for chemistry simulation [22] and QAOA for combinatorial optimization [23], their ansatzes are generated by matrix exponentials, as these better describe the systems to be simulated or the problems encoded in the Hamiltonians. For instance, the recent demonstration of quantum utility [24] is also based on this concept.

While quantum simulation is an important class of algorithms, the circuit consists of a relatively large number of basis gates. For example, the UCCSD ansatz [14] for quantum chemistry simulation requires  $O(n^4)$  Pauli strings and the circuit is typically too large for running meaningful system sizes on current quantum devices. Quantum simulation circuits can be optimized by reordering the Pauli strings to maximize gate cancellation [25], [26], simultaneously diagonalizing the building blocks to reduce gate count [27]–[29], or directly synthesizing a Pauli network [30]. However, the limitation of many existing works is that they rely on local rewriting or synthesizing techniques without leveraging the properties of the quantum simulation circuits. Additionally, many of these optimizations preserve the unitary matrix of the circuit. In this work, we demonstrate that not all gate operations need to be executed on quantum devices. Specifically, operations such as Clifford gates can be efficiently processed classically.

In this paper, we propose a framework that converts quantum simulation programs to hybrid programs, i.e., converting a quantum circuit into a smaller quantum circuit with classical post-processing. This framework, named QuCLEAR (Quantum CLifford Extraction and AbsoRption), significantly reduces the number of two-qubit gates and circuit depth

through two novel optimization techniques: Clifford Extraction and Clifford Absorption. Leveraging the properties of quantum simulation circuits, we propose Clifford Extraction which extracts the Clifford subcircuits to the end of the circuit while optimizing the circuit. The extracted Clifford subcircuits at the end can be efficiently simulated classically. We propose Clifford Absorption which processes the Clifford subcircuits classically by updating the measurement observables or efficiently post-processing the measurement probabilities. QuCLEAR follows a modular design which ensures its portability across different software and hardware platforms. Our experimental comparisons using comprehensive benchmarks demonstrate that QuCLEAR outperforms the state-of-the-art approaches in terms of both gate count and circuit depth.

Our contributions are listed as follows:

- We introduce QuCLEAR, a framework that optimizes quantum circuits. Experimental results across various benchmarks show that QuCLEAR achieves up to a 77.7% reduction in CNOT gate count and up to an 84.1% reduction in entangling depth compared to state-of-the-art methods.
- We propose the technique Clifford Extraction which optimizes quantum circuits. Additionally, we introduce an efficient heuristic algorithm for synthesizing CNOT trees to be extracted in quantum simulation circuits.
- We propose the technique Clifford Absorption which processes the Clifford gates at the end of the circuit classically by updating the measurement observables or post-processing the measurement probabilities.

This paper is organized as follows. In Section II, we introduce the background and the state-of-the-art works. In Section III, we discuss the motivation and key observations. Section IV introduces the high-level design of the QuCLEAR framework. In Section V, we present the algorithm for the Clifford extraction technique. In Section VI, we present the proof and the algorithm for the Clifford absorption technique. In Section VII, we provide our experimental methodology. In Section VIII, we discuss our compilation results and benchmark comparisons. Section IX concludes the paper.

## II. BACKGROUND

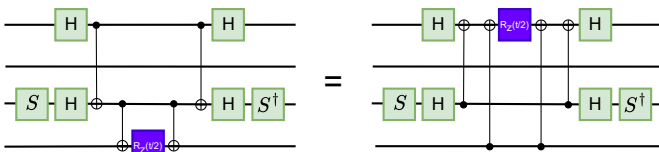


Fig. 1. Equivalent quantum simulation circuits for  $e^{iZYIXt}$

### A. Quantum Simulation

Quantum computation has the potential to benefit solving practical physics and chemistry problems [31]. Two major applications that have been studied are i). solving the eigenvalue and eigenvector of (static) many-body Hamiltonian  $\hat{H}$

and ii). performing Hamiltonian simulation  $e^{-i\hat{H}t}$ . The former can be achieved using variational quantum algorithms by optimizing a parameterized quantum circuit, also known as ansatz [14]. One popular type of ansatz is the chemically-inspired ansatz [32], which involves the exponentiation of qubit-encoded fermionic excitations, e.g.,  $\Pi_{\text{exc}} e^{-i\theta P_{\text{exc}}}$ , where  $P_{\text{exc}}$  is the qubit operator (written in Pauli products) and  $\theta$  is the variational parameter. The latter requires implementing  $e^{-i\hat{H}t}$  on quantum circuits, which can be approximated through Trotterization  $e^{-i\hat{H}t} \approx [\Pi_j e^{-ih_j P_j \Delta t}]^{t/\Delta t}$ , where we've encoded the Hamiltonian into qubits as  $\hat{H} = \sum_j h_j P_j$  and  $\Delta t$  is the timestep. Interestingly, both solutions adopt quantum circuits that share a similar building block  $e^{-i\theta P}$ , that is depicted in Fig. 1. What's more, a similar structure can be extended to QAOA optimization problems. Therefore, optimizing quantum circuits with this building block would benefit a broad range of applications and also improve the practicality of quantum computation on not only near-term but also fault tolerant hardware.

### B. Clifford Circuits

Clifford circuits are a specific class of quantum circuits composed of operations from the Clifford group, which typically includes Hadamard gate  $H$ , Phase gate  $S$ , and CNOT gate [33]. A key feature of Clifford circuits is that they can be efficiently simulated on classical computers. The Gottesman-Knill theorem [34] states that any quantum circuit consisting solely of Clifford gates can be simulated in polynomial time on a classical computer. Although Clifford unitary matrices are  $2^n \times 2^n$  in size, they can be compactly represented using the stabilizer tableau formalism, which requires only  $4n^2 + O(n)$  classical bits to store [35]. An interesting aspect of quantum simulation circuits is that each building block, as shown in Figure 1, typically consists of a single-qubit non-Clifford  $R_z$  rotation sandwiched between two Clifford subcircuits. This structure implies that many operations within these circuits can be efficiently simulated classically, which is crucial for our optimization strategies.

### C. Prior Works

Due to its importance, many works have been proposed to optimize quantum simulation circuits. The prior works can be classified into three categories: Simultaneous Diagonalization [27]–[29], Gate Cancellation [25], [26], [36], [37], and Pauli Network Synthesis [30], [38], [39].

**Simultaneous Diagonalization** Early works on optimizing quantum simulation circuits are based on the simultaneous diagonalization of commuting Pauli strings. While there are many Pauli strings that commute with each other, the Pauli strings can be partitioned into mutually commuting clusters and the strings in each cluster can be simultaneously diagonalized to reduce the circuit cost and also maximize the cancellation between Pauli strings. The T|ket> compiler [40] leverages simultaneous diagonalization [28] and Phase Gadget Synthesis [27] to optimize the circuits.

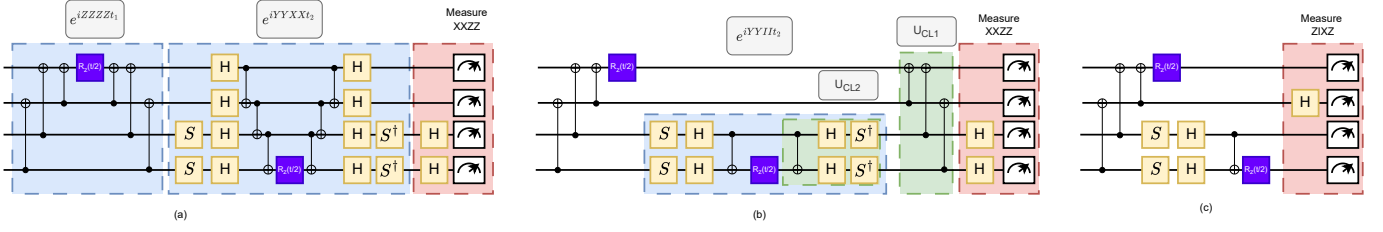


Fig. 2. Optimizing quantum simulation circuit  $e^{iZZZZt_1}e^{iYYXXt_2}$ . (a) The original quantum simulation circuit, which can not be optimized with gate cancellation. The observable that being measured is  $XXZZ$ . (b) The circuit after extracting the Clifford subcircuit in  $e^{iZZZZt_1}$ . The second Pauli rotation circuit is optimized to  $e^{iYYII t_2}$ . (c) Circuit after absorbing the Clifford subcircuit in the observable measurement. The new observable is  $ZIXZ$ .

**Gate Cancellation** The gates in Pauli string subcircuits can be cancelled between two similar Pauli strings. Li et al. [36] propose a software and hardware co-optimization approach to synthesize circuits according to hardware constraints. The followup work Paulihedral [25] generalizes gate cancellations and hardware-aware synthesis by proposing the Pauli Intermediate Representation (IR). Experimental results show that it outperforms simultaneous diagonalization-based methods. Jin et al. propose Tetris [26], which introduces a refined IR that better considers gate cancellation and SWAP gate insertion when synthesizing for devices with limited connectivity.

**Pauli Network Synthesis** The synthesis of quantum simulation circuits can be converted to the synthesis of a Pauli network, which is a generalization of the parity network [41]. Brugière et al. propose Rustiq [30], an efficient approach for synthesizing quantum simulation circuits using Pauli networks. Unlike the symmetric structure in Paulihedral, where each CNOT tree is followed by an inverted CNOT tree to revert the transformations, Rustiq employs a bottom-up synthesis approach to find the smallest Clifford circuits to implement a Pauli string. Schmitz et al. [39] propose mapping a given Hamiltonian simulation circuit to a constrained path on a graph, referred to as the Pauli Frame Graph (PFG). Although interpreted differently, both works use Clifford circuits to transition from one Pauli string to another. The resulting circuit can also be viewed as a Pauli network. Paykin et al. propose PCOAST [38], a generalized compiler optimization framework based on the PFG approach, which has been integrated into the Intel Quantum SDK [42].

In our evaluation, we compare with the state-of-the-art works from all three categories.

### III. MOTIVATION

In this section, we discuss the key observations for our optimizations in the paper. Given that Clifford circuits can be simulated classically, a relevant question arises: Can we optimize quantum circuits by isolating the Clifford subcircuits and simulating them classically? Our optimizations leverage the unique properties of both Clifford circuits and quantum simulation circuits to achieve this goal.

**Clifford circuits and quantum simulation circuits** An important property of quantum simulation circuits is that the circuit for implementing an exponentiated Pauli string (i.e., a Pauli rotation circuit) weakly commutes with Clifford gates.

To understand this weak commutation, consider that Clifford circuits stabilize the Pauli group. In other words, given a Pauli string  $P_1$ , the operation  $U_{CL}^\dagger P_1 U_{CL}$  results in another Pauli string  $P_2$ . Therefore, for a Pauli rotation  $e^{iP_1 t}$  and a Clifford circuit  $U_{CL}$ , we have  $e^{iP_1 t} U_{CL} = U_{CL} e^{iP_2 t}$ , where  $P_2 = U_{CL}^\dagger P_1 U_{CL}$ . As shown in Figure 3, after switching the position of a Clifford circuit with a Pauli rotation, the resulting circuit is another Pauli rotation but with a different Pauli string  $P_2$ . Note that  $P_2$  may include a negative sign. We omit this discussion here for simplicity. However, in our implementation, we track the sign, as it affects the sign of the rotation angle:  $e^{i(-P)t} = e^{iP(-t)}$ .

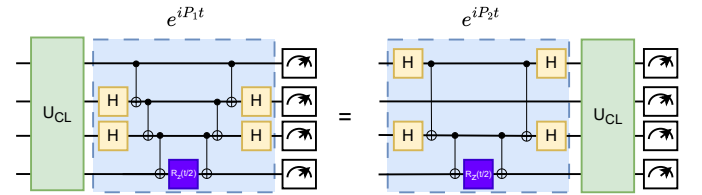


Fig. 3. Clifford circuits weakly commutes with Pauli rotation circuits, meaning that interchanging their positions transforms the Pauli string  $P_1$  to another Pauli string  $P_2$ .

This observation leads to our first optimization design, Clifford Extraction. We can select appropriate Clifford subcircuits and commute them with the Pauli rotations in a circuit. The extracted Clifford circuit can originate from a preceding Pauli rotation circuit. Here we show a simple optimization example in Figure 2. The circuit represents  $e^{iZZZZt_1}e^{iYYXXt_2}$  and we measure the observable  $XXZZ$ . Since these two Pauli strings do not share common Pauli operators, the gate cancellation method in Paulihedral and Tetris can not optimize the circuit. As illustrated in Figure 2(a) and (b), the Clifford subcircuit  $U_{CL1}$  in  $e^{iZZZZt_1}$  can be extracted to the end of the circuit. This extraction simplifies the second Pauli rotation circuit to  $e^{iYYII t_2}$ , reducing the total CNOT gate count from 12 to 8. It also moves the Clifford subcircuits to the end, which is beneficial for subsequent Clifford Absorption optimization.

**Clifford circuits and measurements** In this paper we propose two different approaches for absorbing Clifford subcircuits into measurements and classical post-processing. In many algorithms such as VQE for chemistry simulation, the focus is on measuring the expectation value of a set of Pauli

observables  $O_1, \dots, O_n$ , rather than measuring the probability distribution. Non-Pauli observables can be decomposed into a sequence of Pauli observables. For these observable measurements, we can optimize the circuit by absorbing the Clifford subcircuits into the measurement observables. Figure 4(a) illustrates the high-level idea. Considering a circuit  $U$  with Clifford subcircuit  $U_{CL}$  at the end. Since Clifford circuits stabilize the Pauli group, the measured expectation value of an observable  $O_1$  can be expressed as:  $\langle 0 | U^\dagger U_{CL}^\dagger O_1 U_{CL} U | 0 \rangle = \langle 0 | U^\dagger O_1' U | 0 \rangle$ . Thus, the result is equivalent to removing the Clifford subcircuit and measuring a new Pauli observable  $O_1' = U_{CL}^\dagger O_1 U_{CL}$ . In Figure 2(b) and (c), the two extracted Clifford subcircuits are at the end can be optimized while changing the observable from XXZZ to ZIXZ. By combining Clifford extraction and absorption, we reduce the total CNOT gate count from 12 to 4.

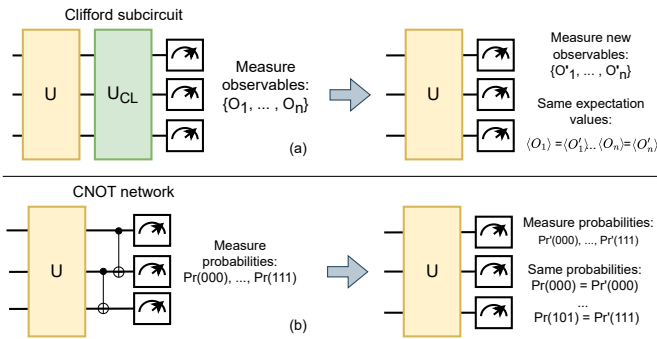


Fig. 4. (a) The Clifford subcircuit at the end can be absorbed into the observable measurements. (b) The CNOT network at the end can be absorbed into the probability measurements.

While chemistry simulation problems typically require measurements of observables, solving combinatorial optimization problems, such as using QAOA for MaxCut, require measuring probabilities in the computational basis. For circuits that require probability distribution, we can consider a simplified case of Clifford subcircuits that consist solely of a CNOT network at the end of the circuit. The CNOT network is essentially a sequence of CNOT gates applied across multiple qubits. As we know, the CNOT gate transforms one computational basis state into another. For example  $CNOT_{0,1} |10\rangle = |10\rangle$ . By measuring the probability distribution before the CNOT network, we can efficiently calculate the output state after the CNOT network. This can also be explained using the principle of deferred measurement [33]; in other words, measurement operations commutes with conditional operations. This approach allows optimizing the CNOT network. As we will demonstrate in Section VI, the Clifford subcircuit in QAOA for combinatorial optimizations can be reduced to a single layer of Hadamard gates and a CNOT network.

Clifford extraction and Clifford absorption techniques complement each other effectively. In the next section, we will introduce the QuCLEAR framework, which integrates these two methods. It is important to note that updating the Pauli strings and calculating the new observables involve multiplying the

Clifford circuits with Pauli operators. These calculations can be performed efficiently on a classical computer using the stabilizer tableau method [34], [43].

#### IV. QUCLEAR FRAMEWORK

In this section, we present a high-level overview of the QuCLEAR framework. Designed in a modular fashion to ensure portability and compatibility across different platforms, the QuCLEAR framework comprises three main components: the Clifford Extraction (CE) module, the Clifford Absorption pre-process (CA-Pre) module, and the Clifford Absorption post-process (CA-Post) module.

Figure 5 shows the QuCLEAR workflow. The process begins with the Clifford Extraction (CE) module that optimizes the input circuit  $U$  into an optimized circuit  $U'$  followed by a Clifford subcircuit  $U_{CL}$ . This step preserves the unitary matrix of the original program,  $U = U_{CL}U'$ . Next, the optimized circuit  $U'$  and the Clifford subcircuit  $U_{CL}$  are passed to the Clifford Absorption pre-process (CA-Pre) module. The CA-Pre module also accepts the observables to be measured as input; if no observables are provided, it defaults to targeting the probability distribution. The CA-Pre module calculates the updated observables and appends the appropriate measurement basis to the end of the circuit. The optimized circuit  $U'$  is then executed on quantum devices using any quantum software stack and hardware, as the framework is platform and software independent. After measuring the probability distribution from the quantum devices, the results are post-processed with the Clifford Absorption post-process (CA-Post) module. For experiments involving observable measurements, the CA-Post module provides the correct mapping between the original observables and the updated ones. For experiments focusing on probability measurements, the CA-Post module identifies the CNOT network at the end and calculates the mapping between the original probabilities and the measured probabilities.

#### V. CLIFFORD EXTRACTION

The Clifford extraction technique extracts Clifford subcircuits to the end of the circuit and optimizes each Pauli string it passes through. For a quantum simulation circuit  $e^{iP_n t_n} \dots e^{iP_1 t_1}$ , we can sequentially extract the right Clifford subcircuits from each Pauli rotation subcircuit (see quantum simulation subcircuit Fig. 1). Starting with the first Pauli  $P_1$  and proceeding to the last Pauli  $P_n$ , this process effectively moves roughly half of the quantum simulation circuit's components to the end. However, extracting Clifford subcircuits is not always advantageous, as the number of non-identity operators may increase after updating the Pauli strings. In this section, we propose a heuristic algorithm for identifying the Clifford subcircuit structure to best optimize the circuit.

##### A. CNOT Tree Synthesis

There are various circuit structures available for synthesizing a Pauli rotation  $e^{iP t}$ . As shown in Figure 1, the Pauli rotation circuit consists of an Rz rotation gate sandwiched

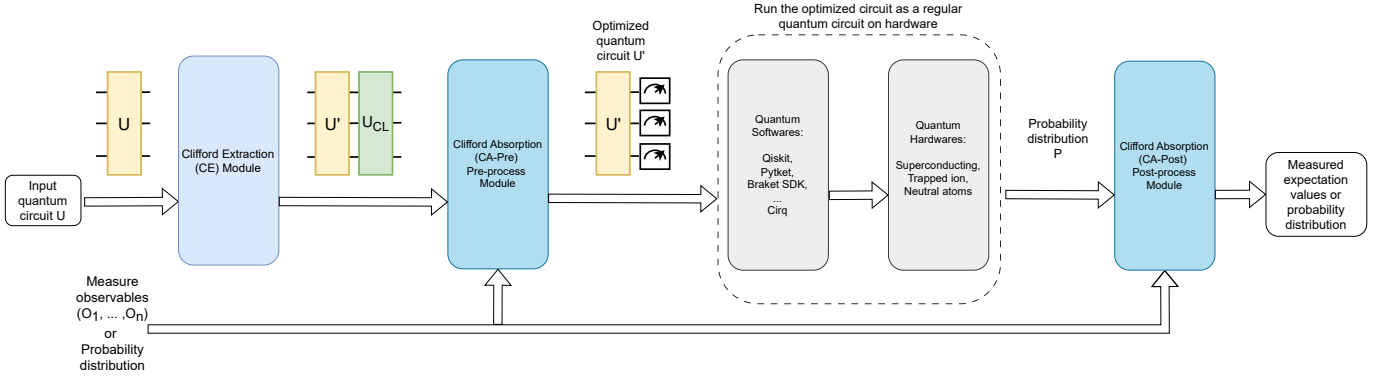


Fig. 5. Overview of the QuCLEAR framework

between mirrored Clifford subcircuits. The Clifford subcircuit includes a layer of single-qubit Clifford gates and a CNOT tree, where the root is the Rz rotation. The CNOT tree is essentially a parity tree, with the root qubit encoding the parity of the state. The placement of the single-qubit Clifford gates is fixed, as it is determined by the Pauli string. However, the synthesis of the CNOT tree structure can vary. First, any qubit can serve as the root qubit. Second, once the root qubit is determined, the CNOT tree can be arranged to connect all the qubits associated with non-identity operators. Although different CNOT tree structures contain the same number of CNOT gates, their resulting unitaries differ, leading to varying optimization capabilities. The task is to identify the best structure for the Clifford extraction.

We first consider a simplified case, focusing on commuting a CNOT gate with a two-qubit Pauli string. The original Pauli  $P$  and the new Pauli  $P'$  after commute are listed in Table I. As shown in the table, the four Pauli strings  $XX$ ,  $YX$ ,  $ZY$ , and  $ZZ$  can be optimized.  $XX$  and  $ZZ$  are special cases where the pattern can be extended to multiple qubits. An  $n$ -qubit Pauli string with all  $Z$  operators  $ZZ\dots ZZ$ , can be optimized by commuting with a chain of CNOT gates to generate a Pauli string with only one non-identity operator:  $II\dots IZ$ . Similarly, an  $n$ -qubit Pauli string with all  $X$  operators  $XXXX\dots X$ , can also be optimized by commuting with a chain of CNOT gates to generate a Pauli with  $\lceil \frac{n}{2} \rceil$  non-identity operators:  $XIXI\dots X$ . An  $n$ -qubit Pauli string with all  $Y$  operators  $YYYY\dots Y$ , can be commuted with a chain of CNOT gates to generate a Pauli with  $\lceil \frac{n}{2} \rceil$  non-identity operators:  $XIXI\dots Y$ . An  $n$ -qubit identity Pauli string  $II\dots I$  remains to be identity after commuting with CNOT gates. The observations lead to our first optimization strategy: grouping identical Pauli operators together.

We will use an example in Figure 6 to demonstrate the process of synthesizing the CNOT tree. The circuit contains three Paulis:  $P_1$ :  $YZXXYZZ$ ,  $P_2$ :  $YZXIZYX$ ,  $P_3$ :  $XZYZIYX$ . Our objective is to find the optimal CNOT tree structure for  $P_1$ , which can optimize  $P_2$  and  $P_3$ . First, since the single-qubit gates are not changeable, we will extract the single qubit gates and update Paulis to  $P_2'$ :  $ZZZIXYX$  and  $P_3'$ :  $YZYXIYX$ . The circuit after extracting the single-qubit gates is shown in

Figure 6(a).

We will find the best CNOT tree structure for optimizing the immediate following Pauli  $P_2'$ . This greedy algorithm is based on the understanding that Pauli operators appearing later in the sequence have more optimization opportunities, as they can be optimized with multiple Clifford subcircuits. Therefore, we prioritize optimizing the first succeeding Pauli string. Based on the observation that identical Pauli operators should be grouped together and processed through a CNOT tree, we first partition the Pauli operators into four groups and synthesize four corresponding subtrees:  $I\_tree$ ,  $X\_tree$ ,  $Y\_tree$ , and  $Z\_tree$ . For the subtrees with multiple nodes, we will use CNOT gates to connect them. When optimizing solely for  $P_2'$ , the order in which qubits are connected within a subtree is unimportant, as their corresponding Pauli operators in  $P_2'$  are identical. Figure 6(b) provides a detailed view of the CNOT tree synthesis. We sequentially connect the qubits within each subtree, designating the last qubit as the root of that subtree. After synthesizing the subtrees, we have four root qubits that need to be connected. According to Table I, we observe that combinations  $YX$  and  $ZY$  can be optimized, while  $IX$  remains unchanged. Therefore we will prioritize connecting the  $Z\_root$  with  $Y\_root$ ,  $I\_root$  with  $X\_root$ , and  $Y\_root$  with  $X\_root$ . The final root qubit is designated as the root for the CNOT tree, where we will place the Rz rotation gate. In our example in Figure 6(b), after extracting the synthesized CNOT tree,  $P_2'$ :  $ZZZIXYX$  is optimized into  $IIIXYX$ .

Note that while the order in which qubits are connected within a subtree is irrelevant for optimizing  $P_2'$ , it may become important for subsequent Pauli strings. This consideration leads to the discussion of the recursive algorithm in the next subsection.

### B. Recursive CNOT Tree Synthesis

The CNOT tree can be synthesized by recursively generating the subtrees. When optimizing  $P_2'$ , the two subtrees  $X\_tree$  and  $Z\_tree$  have the freedom of choosing their root qubit and the order of connecting the qubits with the CNOT gates. To find the optimal gate order, we consider the next Pauli  $P_3'$ :  $YZYXIYX$ . For synthesizing the subtree  $Z\_tree$ , the only



TABLE I

THE NEW PAULI  $P'$  AFTER COMMUTING CNOT WITH ORIGINAL PAULI  $P$ . THE LEFT LETTER REPRESENTS THE CONTROL QUBIT AND THE RIGHT LETTER REPRESENTS THE TARGET QUBIT. THE PAULI OPERATORS THAT HAVE BEEN REDUCED ARE MARKED IN **BOLD**.

P	II	IX	IY	IZ	XI	XX	XY	XZ	YI	YX	YY	YZ	ZI	ZX	ZY	ZZ
P'	II	IX	ZY	ZZ	XX	<b>XI</b>	YZ	YY	YX	<b>YI</b>	XZ	XY	ZI	ZX	<b>IY</b>	<b>IZ</b>

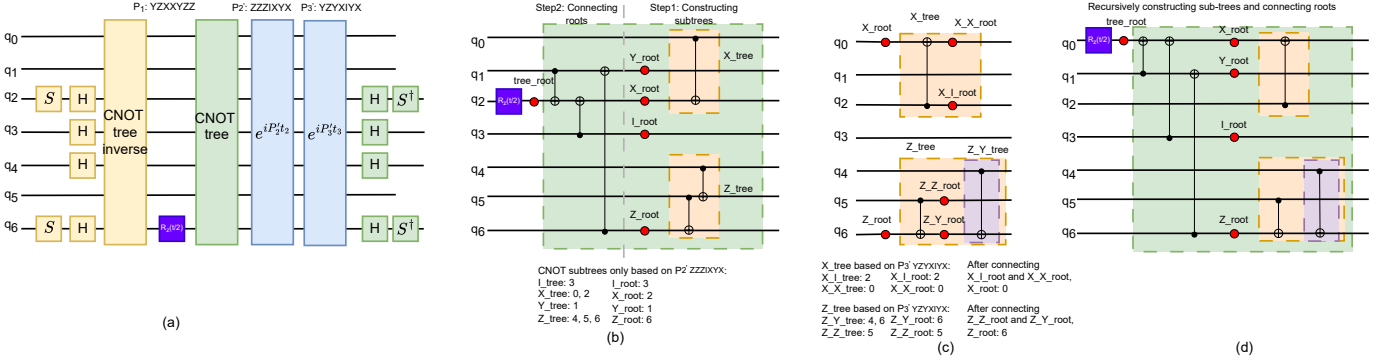


Fig. 6. Synthesizing the CNOT tree circuit for  $P_1$ . (a) Circuit after extracting the single-qubit gates in  $e^{iP_1t}$ . (b) A detailed view of tree circuit synthesis for optimizing  $P_2'$ . (c) The synthesis process for the two subtrees,  $X\_tree$  and  $Z\_tree$  based on  $P_3'$ . (d) The synthesized tree circuit for optimizing  $P_2'$  and  $P_3'$ .

requirement is to connect the three qubits  $q_4$ ,  $q_5$ , and  $q_6$ . Thus, we examine the corresponding three Pauli operators in  $P_3'$  which are  $YZY$ . Figure 6(c) details the synthesis of the two subtrees  $X\_tree$  and the  $Z\_tree$ . For  $Z\_tree$ , we follow the same process: synthesizing subtrees  $Z\_Y\_tree$  and  $Z\_Z\_tree$ . Then connect the root qubits  $Z\_Y\_root$  and  $Z\_Z\_root$  using the previously discussed root connection strategy. This process is equivalent to calling the tree synthesis algorithm with a smaller Pauli substring of  $P_3'$ :  $P_3'[4:7]$ . Therefore, we can recursively call the tree synthesis algorithm to build subtrees and connect the root qubits. The final circuit for optimizing both  $P_2'$  and  $P_3'$  is shown in Figure 6(d). If we extract the CNOT tree in Figure 6(b),  $P_3'$   $YZYXIYX$  will be converted into  $IXXXYX$  where the number of non-identity operator is not reduced. However, if we extract the optimized CNOT tree in Figure 6(d),  $P_3'$  will be optimized into  $IIXXIYX$ , converting two non-identity operators into identity operators.

The recursive algorithm for synthesizing a CNOT tree is outlined in Algorithm 1. The input is the Pauli string for synthesis. The  $p\_idx$  is the index of the Pauli to be synthesized. The  $qc$  is the quantum circuit to add CNOT gates. The  $tree\_idxs$  is the list of indexes of the current tree.  $extr\_clf$  is the already extracted Clifford circuit, which will be used to calculate the updated Pauli  $U_{CL}^\dagger P U_{CL}$ . After initializing all the variables, we will find the next Pauli string and use  $update\_pauli$  function to calculate the updated next Pauli. For every qubit index in  $tree\_idxs$ , we examine the corresponding Pauli operator in the next Pauli string  $next\_pauli$  and append the qubit index to the appropriate subtree. Then we evaluate each subtree. If a subtree contains only one qubit, we designate it as the  $subtree\_root$ . Otherwise, we need to determine the order of the CNOT gates for that subtree. We recursively call the  $tree\_synthesis$  algorithm to construct the subtree and return the  $subtree\_root$ . Once all the subtrees are generated, we

connect the roots in sequence. The function  $connect\_roots$  is invoked to add CNOT gates to the quantum circuit  $qc$  between the root qubits of the subtrees. The last root becomes the return value of the  $tree\_synthesis$  algorithm.

### C. Clifford Extraction Algorithm

In this subsection, we present our Clifford Extraction algorithm. The pseudo code is listed in Algorithm 2, for simplicity we omit the parameters associated with the Paulis. The algorithm takes a list of Pauli strings as input and outputs the optimized quantum circuit  $opt\_qc$ , and the extracted Clifford circuit  $extr\_clf$ . The algorithm begins with converting the Pauli list  $P$  into blocks of commuting Paulis. These blocks capture local commuting information, allowing Paulis within each block to switch order. This reordering is useful for optimizing the circuit. It is important to note that this approach differs from the block definition in Paulihedral. In QuCLEAR, the Paulis within a block can change order, but the order of the blocks themselves remains fixed. In contrast, Paulihedral allows the block order to change, enabling more global optimization. This difference in design choices stems from our decision not to assume any high-level information or prior knowledge about the benchmarks.

Since Paulis commute within a block, QuCLEAR uses the  $find\_next\_pauli$  function to identify the most suitable Pauli in the current commuting block. The  $find\_next\_pauli$  function traverses the current block, computes the optimized Pauli for each, and selects the Pauli with the fewest non-identity operators after extracting the Clifford from the current Pauli string. The cost associated with each Pauli is determined by running  $tree\_synthesis$  without recursion to compute the optimized Pauli string. After finding the next Pauli, we will use  $tree\_synthesis$  function to recursively generate the CNOT tree and return the root qubit index  $tree\_root$ . Then we will

---

**Algorithm 1** *tree\_synthesis*

---

**Require:** Pauli strings  $P$ , Pauli index  $p\_idx$ , Quantum circuit  $qc$ , Tree indexes  $tree\_idxs$ , extracted Clifford circuit  $extr\_clf$ .

**Ensure:** Append a synthesized CNOT tree to quantum circuit  $qc$  based on the Pauli strings in  $P$ , and return the tree root index  $tree\_root$ .

```
1:  $I\_tree = X\_tree = Y\_tree = Z\_tree = []$ 
2:  $next\_idx = p\_idx + 1$ 
3:  $next\_pauli = update\_pauli(P[next\_idx], extr\_clf)$ 
4: for each  $index$  in  $tree\_idxs$  do
5:   switch  $next\_pauli[index]$  do
6:     case  $X$ : Append  $index$  to  $X\_tree$ 
7:     case  $Y$ : Append  $index$  to  $Y\_tree$ 
8:     case  $Z$ : Append  $index$  to  $Z\_tree$ 
9:     case  $I$ : Append  $index$  to  $I\_tree$ 
10:  end switch
11: end for
12: for each  $subtree$  in  $\{X\_tree, Y\_tree, Z\_tree, I\_tree\}$  do
13:   if  $len(subtree) = 1$  then
14:      $subtree\_root \leftarrow subtree[0]$ 
15:   else if  $len(subtree) > 1$  then
16:      $subtree\_root \leftarrow tree\_synthesis(P, next\_idx, qc, subtree, extr\_clf)$ 
17:   end if
18:   Assign  $subtree\_root$  to the corresponding root variable ( $X\_root, Y\_root, Z\_root, I\_root$ )
19: end for
20:  $all\_roots = (Z\_root, I\_root, Y\_root, X\_root)$ 
21: for each  $root\_name$  in  $all\_roots$  do
22:    $tree\_root \leftarrow connect\_roots(qc, root\_name, all\_roots)$ 
23: end for
24: return  $tree\_root$ 
```

---

update the optimized circuit  $opt\_qc$  and the already extracted Clifford circuit  $extr\_clf$ . After traversing all Paulis in the list  $P$ , we generate the optimized quantum circuit and the extracted Clifford subcircuit  $extr\_clf$ .

During the execution of the algorithm, the  $extr\_clf$  variable keeps track of the already extracted Clifford circuits. This variable is used to update the next Pauli string. Whenever we determine the CNOT tree design, we defer the extraction of the CNOT tree to avoid the overhead of updating all subsequent Pauli strings. Instead, we only update the Pauli string when needed, specifically when it becomes the  $next\_pauli$  in the CNOT tree synthesis process.

#### D. Scaling

The Clifford Extraction algorithm is scalable with respect to both the number of qubits  $n$  and the number of Pauli strings  $m$ . First, converting Paulis into commuting blocks requires comparing each Pauli with every other Pauli and checking each bit, resulting in a worst-case complexity of  $O(nm^2)$  op-

---

**Algorithm 2** Clifford Extraction Algorithm

---

**Require:** List of Pauli strings  $P$ ,

**Ensure:** Synthesize an optimized quantum circuit  $opt\_qc$  and the extracted Clifford circuit  $extr\_clf$ .

```
1:  $commute\_blocks = convert\_commute\_sets(P)$ 
2: for  $block$  in  $commute\_blocks$  do
3:   for  $pauli\_idx$  in  $range(len(block))$  do
4:      $curr\_pauli = block[pauli\_idx]$ 
5:      $next\_idx = find\_next\_pauli(curr\_pauli, pauli\_idx, block, extr\_clf)$ 
6:      $next\_pauli = block.pop(next\_idx)$ 
7:      $block.insert(pauli\_idx + 1, next\_pauli)$ 
8:      $cx\_tree = QuantumCircuit()$ 
9:      $tree\_root = tree\_synthesis(block, pauli\_idx, cx\_tree, extr\_clf)$ 
10:    Update  $opt\_qc$  and  $extr\_clf$  based on the CNOT tree  $cx\_tree$ , the root qubit  $tree\_root$ , and  $curr\_pauli$ .
11:   end for
12: end for
13: return  $opt\_qc, extr\_clf$ 
```

---

erations. Subsequently, for each Pauli, the algorithm searches for the optimal next Pauli within the current commuting block. In the worst-case scenario, where all Paulis commute, the  $tree\_synthesis$  function needs to be called  $O(m^2)$  times. For each  $tree\_synthesis$  run, the maximum recursive depth is  $O(n)$ , and the most time consuming step in each recursive call is to update the Pauli operators with the already extracted Cliffords. Based on the stabilizer tableau [34], [43], the update of the Clifford operators requires only  $O(n^2)$  operations on classical computers. Therefore, the worst-case time complexity of  $tree\_synthesis$  is  $O(n^3)$ , leading to an overall worst-case complexity of  $O(n^3m^2)$ . The algorithm shares the same complexity as the Rustiq algorithm [30]. However, in the best-case scenario, where none of the Paulis commutes, the time complexity is reduced to  $O(n^3m)$ . As demonstrated in our experiments in Section VIII, our approach achieves significantly shorter compile times when the order of the Pauli operators remains relatively unchanged.

#### E. Comparison with Rustiq

After extracting half of the Clifford gates, the circuit can be viewed as a Pauli network in Rustiq, as it contains single-qubit rotation gates and the connecting Clifford operations. The primary difference lies in how the network is constructed. QuCLEAR employs a top-down synthesis approach, where CNOT trees are synthesized based on the Pauli strings. In contrast, Rustiq utilizes a bottom-up synthesis approach, relying on searching for basic Clifford building blocks to identify the optimal Clifford circuits. The top-down synthesis and the recursive algorithm in QuCLEAR allow for further optimization of subsequent Pauli strings. As shown in Section VIII, our results outperform Rustiq and are more scalable for deep circuits. Another key difference is that we leverage the Clifford Absorption technique to optimize the circuits further.

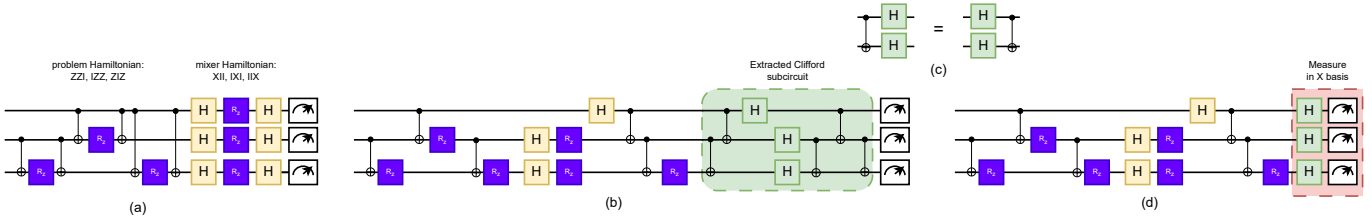


Fig. 7. Optimizing the QAOA circuit with Clifford Absorption. (a) The original QAOA circuit for MaxCut problem. (b) The optimized circuit after Clifford Extraction. (c) A layer of Hadamard gates commutes with CNOT gate. (d) The optimized circuit after absorbing the CNOT network.

## VI. CLIFFORD ABSORPTION

The Clifford Absorption modules behave slightly differently depending on whether observables or probability distributions are being measured. We will discuss each scenario in the following subsections.

### A. Observable Measurement

When applying quantum simulation circuits to simulate chemical systems, the primary research interest is in measuring observables. These observables are typically represented as a set of Pauli strings  $O_1, \dots, O_m$ . For example, an  $n$ -qubit VQE algorithm requires measuring  $O(n^4)$  Pauli observables for molecular Hamiltonians [44], [45]. As discussed in Section III, the Clifford subcircuit  $U_{CL}$  extracted by the Clifford Extraction module can be absorbed into these observables. The new observables are  $O'_i = U_{CL}^\dagger O_i U_{CL}$  which are also Pauli observables. To measure these new Pauli observables, it is necessary to adjust the measurement basis by adding single-qubit rotations at the end of the circuit. The CA-Pre module calculates the new observables and pre-processes the circuits by adding the corresponding single-qubit gates. While our default implementation measures these observables separately (requiring one circuit per observable), it does not preclude the possibility of further optimizations. Due to the property of Clifford operations preserving the commutation and anti-commutation relationships between Pauli operators, the transformed observables retain these relationships. We can apply the commutation-based measurement reduction technique [46] to reduce the number of measurements to  $O(n^3)$  or use the classical shadow [47] to estimate the expectation value of the observables. The CA-Post module for observable measurement is straightforward; it functions as a dictionary, mapping the measurement results to the correct observables.

The CA modules are highly scalable with respect to the number of qubits. The update of the Clifford operators requires only  $O(n^2)$  operations on classical computers. Additionally, it takes  $4n^2 + O(n)$  classical bits [35] to store the stabilizer tableau. For  $k$  observables to measure, the total classical computation overhead of the CA modules is  $O(kn^2)$ .

### B. Probability Distribution Measurement

When solving the combinatorial optimization problem using QAOA, the result is measured in the computational basis, and the classical bitstring corresponds to the solution of the problem. In order to absorb the Clifford gates, one direct

solution is converting the probability measurement of  $2^n$  states to measure  $2^n$  observables. However, that exponentially scales with the number of qubits, which is undesirable.

We propose a scaling approach based on the properties of the QAOA algorithm. In the QAOA, two primary Hamiltonians are employed iteratively: the problem Hamiltonian (also known as the cost Hamiltonian) and the mixer Hamiltonian. These Hamiltonians play distinct roles in encoding the optimization problem and exploring the solution space. Combinatorial optimization problems are encoded in the problem Hamiltonian, which typically consists only of Pauli Z and I operators, as they represent classical terms. For instance, Quadratic Unconstrained Binary Optimization (QUBO) [48] problems can be expressed as a sequence of Pauli Z and ZZ rotations in QAOA. Other combinatorial optimization problems, such as Low Autocorrelation Binary Sequences (LABS) [49], [50], might require more multi-qubit Pauli Z rotations. The mixer Hamiltonian ensures that the quantum state does not get trapped in local minima and can explore different configurations. It typically consists of  $n$  Pauli strings with a Pauli X rotation acting on each qubit.

Figure 7(a) illustrates a single-layer QAOA circuit for the MaxCut problem. The problem Hamiltonian is  $ZZI + IZZ + ZIZ$  and the mixer Hamiltonian is  $XII + IXI + IIX$ . We can extract the Clifford subcircuit using the Clifford Extraction technique and the resulting circuit is shown in Figure 7(b). Since the original Hamiltonians only contain Pauli I, X, and Z operators, the extracted Clifford circuit only consists of Hadamard gates and CNOT gates. By leveraging the circuit equivalence shown in Figure 7(c), we can commute the Hadamard gates with the CNOT gates. The Clifford subcircuit is equivalent to a single layer of Hadamard gates and a CNOT network, which can be classically simulated. When resolving the CNOT network classically, the complexity depends on the number of shots used to collect the probability distribution. This approach significantly reduces the computational overhead, as the complexity no longer scales exponentially with the number of qubits. We will provide a detailed scalability analysis in the following paragraph. The final optimized circuit is shown in Figure 7(d), where the single-layer of Hadamard gates at the end is equivalent to measuring all the qubits in the Pauli X basis. The CNOT gate count is reduced from 6 to 5. While the reduction of just one CNOT gate may seem minor, the previous circuit was already highly optimized, and any improvement is valuable. We will demonstrate in Section VIII



that for larger circuits and more complicated problems, the reduction in gate count becomes more significant.

In this Section, we prove that the Clifford subcircuit extracted in the QAOA algorithm can be optimized to a single layer of Hadamard gates followed by a CNOT network.

**Proposition 1.** *In the QAOA algorithm, for any problem Hamiltonian consisting only of Pauli I and Z operators and a mixer composed of Pauli X rotations, the extracted Clifford subcircuit can be reduced to a single layer of Hadamard gates and a CNOT network.*

To establish this result, we define a sequence of Pauli strings consisting solely of Pauli Z and I operators as a Z-I Pauli sequence. In the QAOA algorithm, the problem Hamiltonian consists of Z-I Pauli sequences, while the mixer Hamiltonian consists of X-I Pauli sequences. We then present the following lemma:

**Lemma 1.** *Commuting a CNOT network with a Z-I Pauli sequence results in a new Z-I Pauli sequence. Commuting a CNOT network with an X-I Pauli sequence results in a new X-I Pauli sequence.*

This can be straightforwardly demonstrated by noting that a single CNOT gate transforms a Pauli string containing Z and I operators into another Pauli string of the same type, and the same logic applies to X-I Pauli sequences. Based on Lemma 1, the Clifford subcircuit extracted from a Z-I Pauli sequence is a CNOT network since each Z-I Pauli string, when commuted with the CNOT network, results in another Z-I Pauli string. The extracted Clifford circuit will only contain CNOT gates.

The mixer Hamiltonian consists of an X-I Pauli sequence. Commuting a CNOT network with the mixer Hamiltonian generates a new X-I Pauli sequence. When performing Clifford extraction for the updated mixer layer, we extract a CNOT network and a layer of Hadamard gates. The extracted Hadamard layer converts the next Z-I Pauli sequence into an X-I Pauli sequence, and the CNOT network subsequently transforms the X-I Pauli sequence into another X-I Pauli sequence. Therefore, for a QAOA algorithm with  $j$  layers of problem and mixer Hamiltonians, the extracted Clifford subcircuit consists of  $2j - 1$  layers of Hadamard gates and  $2j$  layers of CNOT networks. As shown in Figure 7(b), the extracted circuit consists of one layer of Hadamard gates and two layers of CNOT networks. The Hadamard layers can be merged into a single layer, resulting in a final extracted circuit composed of a single layer of Hadamard gates followed by a CNOT network at the end.

When measuring probability distributions, the CA-Pre module adds a single layer of Hadamard gates at the end of the optimized circuit. The CA-Post module will calculate the updated probability distribution based on the measured probabilities and the CNOT network.

The calculation of the CA-Post module is also scalable. The simulation of a single CNOT gate involves only an XOR operation, which is an  $O(1)$ . Considering a QAOA problem with  $k$  shots and measured  $s$  states with non-zero probability,

only these  $s$  states need to be updated, rather than the total  $2^n$  states.  $s$  should always be smaller than or equal to the number of shots  $k$ . In the worst case, where each measured state corresponds to a unique shot, and there are  $m$  CNOTs in the CNOT network, the classical computation overhead of the CA module is  $O(mk)$ . In practice, the number of shots is typically a constant number, such as 1000.

## VII. METHODOLOGY

**Benchmarks:** We evaluate 19 benchmarks in our experiments, including different sizes and applications. For the chemistry eigenvalue problem, we select the UCCSD ansatz using the Jordan-Wigner transformation [51] with different number of electrons and orbitals. For instance, UCC-(2,4) refers to a configuration with two electrons and four spin orbitals, representing a valid active space for simulating  $H_2$ . We also include the Hamiltonian simulation for LiH,  $H_2O$ , and the benzene molecule, with well-established active spaces [52], [53]. For the combinatorial optimization problems, we select the QAOA algorithm for solving MaxCut problems on regular graphs of degrees 4, 8, 12, and random graphs. MaxCut-(n15, r4) refers to regular graph with 15 nodes, each having a degree of 4. MaxCut-(n15, e63) refers to random graph with 15 nodes and 63 edges. Additionally, we evaluate the QAOA for solving Low Autocorrelation Binary Sequences (LABS) problems, which have recently demonstrated a scaling advantage over classical algorithms [50]. The QAOA for LABS problem contains multi-qubit Pauli Z rotations in the problem Hamiltonian. All the QAOA benchmarks contain one iteration of the problem and mixer Hamiltonian. The benchmarks and the native number of gates, without any optimizations, are listed in Table II.

TABLE II  
BENCHMARK INFORMATION

Type	Name	#qubits	#Pauli	#CNOT	#1Q
UCCSD	UCC-(2,4)	4	24	128	264
	UCC-(2,6)	6	80	544	944
	UCC-(4,8)	8	320	2624	3968
	UCC-(6,12)	12	1656	18048	21096
	UCC-(8,16)	16	5376	72960	69120
	UCC-(10,20)	20	13400	217600	173000
Hamiltonian simulation	LiH	6	61	254	421
	$H_2O$	8	184	1088	1624
	benzene	12	1254	10060	12390
QAOA LABS	LABS-(n10)	10	80	340	100
	LABS-(n15)	15	267	1316	297
	LABS-(n20)	20	635	3330	675
QAOA MaxCut	MaxCut-(n15, r4)	15	45	60	75
	MaxCut-(n20, r4)	20	60	80	100
	MaxCut-(n20, r8)	20	100	160	140
	MaxCut-(n20, r12)	20	140	240	180
	MaxCut-(n10, e12)	10	22	24	42
	MaxCut-(n15, e63)	15	78	126	108
	MaxCut-(n20, e117)	20	137	234	177

#1Q denotes the number of single-qubit operations

**Implementation:** We prototype our QuCLEAR framework in Python3.10 on top of the quantum computing framework Qiskit [54].

**Comparison with state-of-the-art methods :** We compared QuCLEAR with Qiskit version 1.1.1 [54], T|ket) version

1.30.0 [27], Paulihedral [25], and Rustiq [30]. The baselines encompass a range of methods. T|ket) employs the simultaneous diagonalization method [27], [28]. Paulihedral focuses on gate cancellation. Rustiq employs Pauli network synthesis. In our experiments we target the compilation on a fully-connected device. We did not compare with Tetris [26] as it specifically optimizes for devices with limited connectivity. All the baselines have been updated to the latest versions available at the time of writing this paper. QuCLEAR and Paulihedral are optimized with Qiskit optimization level 3. T|ket) is optimized with its own optimization pass with maximum optimization setting O2. We didn't optimize T|ket) circuits with Qiskit optimization passes as previous research [26] indicates that T|ket) performs best with its own optimizer. Rustiq is not further optimized because the Rustiq-optimized circuit only outputs the Pauli network and omits the single-qubit Rz rotation gates. We choose the *rcount* implementation in Rustiq to minimize the CNOT gate counts.

We compared the CNOT gate count, the entangling depth (also known as CNOT-depth), and the compile time across different methods. We compared the entangling depth instead of the circuit depth to ensure a fair comparison, as Rustiq's results do not include the single-qubit rotation gates. The evaluations were performed on a Windows 10 device with an Intel Core i7-10870H CPU @2.20GHz, NVIDIA GeForce RTX 3080 Laptop GPU, 32.0GB RAM, and 1TB SSD.

## VIII. EVALUATION

### A. Comparison with the State-of-the-art Works

Table III shows the CNOT gate count, entangling depth, and the compilation time on a fully connected device. The best results are marked in bold. In summary, QuCLEAR can reduce the CNOT gate count by up to 68.1% (50.6% average), 52.5% (31.5% average), 63.9% (43.1% average), 77.7% (49.3% average) compared to Qiskit, Rustiq, Paulihedral, and T|ket), respectively. QuCLEAR can reduce the entangling depth by up to 80.2% (58.7% average), 53.6% (36.0% average), 76.2% (51.2% average), and 84.1% (59.1% average) compared to Qiskit, Rustiq, Paulihedral, and T|ket), respectively.

**CNOT gate count** QuCLEAR produces the fewest CNOT gates in 16 out of 19 benchmarks. The reduction in CNOT gates is particularly significant for the chemistry simulation benchmarks. This is because these benchmarks involve more complex Pauli strings, whereas the combinatorial optimization problems have Pauli strings in a more uniform format. Our recursive tree synthesis algorithm provides a greater advantage in optimizing the complex Pauli strings. The three cases where QuCLEAR does not produce the best results are the MaxCut problems with relatively sparsely connected graphs. In our optimization process, extracting the Cliffords through the mixer layer converts the single-qubit Rx rotations into multi-qubit rotations as shown in Figure 7(b). In other words, while we simplify the circuit in the problem Hamiltonian layer, we inadvertently increase the complexity in the mixer layer. Therefore, our approach is more advantageous for more complex problems, such as MaxCut graphs with higher-order

connections or the LABS problem. For the 20-qubit MaxCut problems with 8- or 12-regular graphs, our compiler is the only one that achieves a non-trivial reduction in CNOT gate count compared to the original circuit.

**Entangling depth** QuCLEAR produces the circuits with shortest entangling depth for all the chemistry simulation benchmarks and two of the LABS benchmarks, with the third LABS comparison being very close to the best. This result aligns with our previous discussion. Although minimizing circuit depth is not our primary target, extracting the Clifford subcircuit inherently reduces the circuit depth. For instance, in a standard V-shaped quantum simulation circuit, extracting half of the CNOTs effectively cuts the circuit depth in half. The extraction of the Clifford circuits and the consequent reduction in the CNOT gate count contribute significantly to the decreased entangling depth. However, for the MaxCut benchmarks, increasing the complexity in the mixer layer leads to a greater circuit depth and may result in long chains of CNOT gates, which can increase the overall circuit depth.

**Compile time** Among all the methods, Rustiq has the shortest compile time for most of the benchmarks, owing to its implementation in Rust [55]. In contrast, our implementation is in Python. For the chemistry simulation benchmarks, the runtime of QuCLEAR with Qiskit optimization level 3 is very close to the runtime of Qiskit alone. The significant reduction in circuit size shortens the runtime for Qiskit's optimization. Notably, for the largest benchmark, UCC-(10,20), QuCLEAR achieves the best compile time, being orders of magnitude faster than Rustiq. For the QAOA problems, QuCLEAR experiences longer compile times due to the search required within the commuting blocks. Despite this, it still manages to achieve compile times comparable to T|ket).

We also present the QuCLEAR results and runtime without applying Qiskit optimization. As shown in Figure 8, the Qiskit optimization does not reduce the CNOT counts for the QAOA benchmarks. Applying Qiskit optimizations results in an average CNOT count reduction of 4.4% and increases the compile time by 6%. This confirms that our framework is effective on its own.

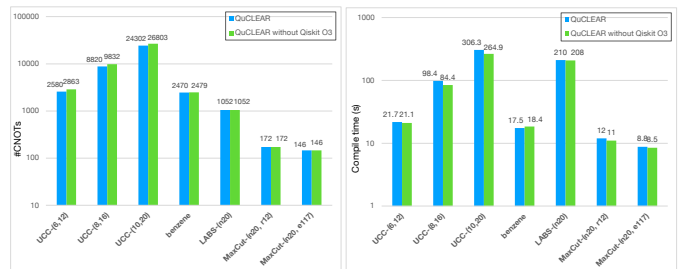


Fig. 8. Comparison of QuCLEAR with and without Qiskit optimization

### B. Clifford Absorption Runtime

The runtime of the Clifford Absorption (CA) module scales linearly with the number of observables or states. We measured

TABLE III  
RESULTS AND COMPILE TIME COMPARED WITH THE STATE-OF-THE-ART WORKS ON A FULLY CONNECTED DEVICE.

Name	#CNOT					Entangling depth					Compile time (s)				
	QuCLEAR	Qiskit	Rustiq	PH	tket	QuCLEAR	Qiskit	Rustiq	PH	tket	QuCLEAR	Qiskit	Rustiq	PH	tket
UCC-(2,4)	<b>23</b>	41	33	48	53	<b>17</b>	41	31	48	50	0.1327	0.1546	<b>0.001</b>	0.1356	2.2191
UCC-(2,6)	<b>106</b>	181	161	216	236	<b>82</b>	178	145	215	211	0.561	0.5823	<b>0.007</b>	0.5864	9.2433
UCC-(4,8)	<b>448</b>	1003	795	947	1257	<b>335</b>	990	666	941	1112	3.0018	2.5905	<b>0.0848</b>	3.2474	49.1337
UCC-(6,12)	<b>2580</b>	5723	4705	6076	8853	<b>1832</b>	5582	3588	6051	7924	21.656	19.6461	<b>10.7976</b>	24.1745	365.9686
UCC-(8,16)	<b>8820</b>	23498	18552	23389	36369	<b>6153</b>	23020	13092	23333	33074	98.4158	<b>96.1222</b>	759.8567	137.9728	2224.6543
UCC-(10,20)	<b>24302</b>	72005	50913	67336	109130	<b>15979</b>	70705	34403	67237	100585	<b>306.3307</b>	342.6219	14802.1183	629.8874	14278.8268
LiH	<b>74</b>	180	114	121	132	<b>60</b>	176	92	119	112	0.3999	0.3701	<b>0.0059</b>	0.3939	5.0096
H <sub>2</sub> O	<b>274</b>	786	350	471	505	<b>189</b>	769	267	461	442	1.7922	1.5299	<b>0.0259</b>	1.4013	18.5444
benzene	<b>2470</b>	7602	3356	3267	4738	<b>1481</b>	7477	2321	3237	4092	18.4479	13.607	<b>4.6286</b>	15.9836	210.8994
LABS-(n10)	<b>106</b>	296	116	230	145	<b>76</b>	173	77	209	127	1.608	0.1553	<b>0.0199</b>	1.9484	4.2117
LABS-(n15)	<b>385</b>	1208	457	880	641	<b>255</b>	672	281	797	568	21.797	0.5156	<b>0.1077</b>	0.4199	21.3482
LABS-(n20)	<b>1052</b>	2914	1138	2218	1762	<b>679</b>	1731	<b>677</b>	2023	1673	210.1475	1.4367	<b>0.5801</b>	1.2457	64.2246
MaxCut-(n15, r4)	68	<b>58</b>	94	60	62	32	28	50	<b>26</b>	36	1.0402	0.0678	0.0399	<b>0.0299</b>	2.092
MaxCut-(n20, r4)	88	<b>78</b>	126	80	100	34	28	60	<b>22</b>	46	2.1981	0.0928	0.0848	<b>0.0399</b>	3.6862
MaxCut-(n20, r8)	<b>129</b>	158	188	160	210	59	94	104	<b>48</b>	123	5.3028	0.1436	<b>0.0888</b>	0.1074	7.6895
MaxCut-(n20, r12)	<b>172</b>	238	218	240	247	93	158	112	<b>70</b>	121	11.0385	0.2613	<b>0.1207</b>	0.1636	8.1801
MaxCut-(n10, e12)	26	<b>22</b>	33	24	24	21	<b>10</b>	18	12	12	0.2882	0.0319	<b>0.009</b>	0.016	0.843
MaxCut-(n15, e63)	<b>93</b>	114	108	102	137	51	<b>36</b>	59	42	69	2.6584	0.6096	<b>0.0389</b>	0.0904	4.4406
MaxCut-(n20, e17)	<b>146</b>	216	188	192	298	65	<b>56</b>	85	<b>56</b>	121	8.4899	0.1715	<b>0.0918</b>	0.2055	10.1784

The results for both QuCLEAR and PH were obtained after applying Qiskit optimization level 3. The compile time represents the total time required for running both QuCLEAR and the Qiskit optimization. PH denotes Paulihedral.

TABLE IV  
CLIFFORD ABSORPTION RUNTIME (S) FOR UCC-(10,20) AND MAXCUT-(N20, R12) BENCHMARKS

Number	10	50	100	500	1000	5000
Observables	0.052	0.268	0.453	2.316	4.539	23.060
States	0.003	0.017	0.032	0.161	0.325	1.675

the runtime separately because it depends not only on the circuit but also on the number of observables or states considered. To illustrate this, we selected the largest chemistry simulation benchmark, UCC-(10, 20), and the numerical optimization benchmark, MaxCut-(n20, r12). The number of CNOT gates in the Clifford circuit is the same as the CNOT counts listed in Table III. We then executed the CA module with varying numbers of observables and states. As shown in Table IV, the runtime scales linearly. For a reasonable number of observables and states, the runtime remains acceptable compared to the overall compile time.

### C. Closer Examination of the Improvements

Since we have introduced several optimizations, it is essential to quantify the contributions. We selected two benchmarks, UCC-(4,8) from the chemistry simulation category and MaxCut-(n20, r8) from the combinatorial optimization category. We present a detailed breakdown of the CNOT gate count reduction achieved by each optimization in Figure 9.

For the chemistry simulation problems, the Pauli strings contain many non-identity Pauli operators. As a result, recursively synthesizing the CNOT tree and extracting the Clifford subcircuit significantly optimize the circuit, reducing the gate count from 2624 to 1014. Since few Pauli strings commute with their neighbors, incorporating commuting considerations only slightly reduces the gate count to 984. The next notable reduction occurs when we absorb the Clifford subcircuits, effectively halving the gate count. And with the local rewriting optimizations in Qiskit, the final gate count is reduced to 448.

The QAOA for MaxCut benchmark exhibits a different pattern. It consists of Pauli strings with only one or two non-identity Pauli operators. Therefore, simply extracting the Clifford circuits can potentially increase the circuit size, as it often results in a greater number of non-identity Pauli operators in the strings. Since many Paulis commute, the commutation optimization reduces the CNOT gate count from 286 to 258. Absorbing the CNOT network also halves the gate count, bringing it down to 129. The subsequent optimizations in Qiskit do not further reduce the gate count.

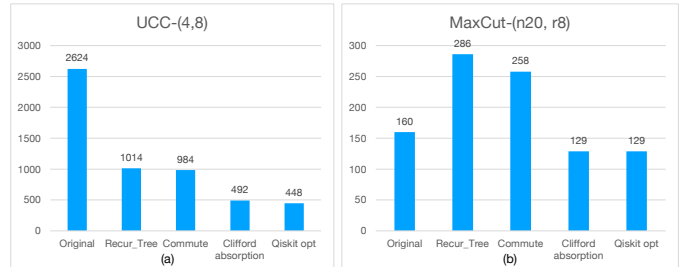


Fig. 9. A breakdown of the CNOT gate reduction achieved by each individual feature in optimizing the UCC-(4,8) and MaxCut-(n20, r8) benchmark.

### D. QAOA Case Study: Increasing layers

As we have discussed, our approach performs better with denser graphs. Given that QAOA often requires multiple layers, we also aim to study the relationship between gate counts and the number of layers. Due to space constraints, we present results for a select set of benchmarks with the number of layers increased to three. The results are shown in Table V. By comparing with the single layer results in Table III, we observe that the number of CNOT gates scales almost linearly with the number of layers. This demonstrates that our approach is effective for optimizing deeper circuits as the number of layers increases.

TABLE V  
QAOA BENCHMARKS WITH THREE COST AND MIXER LAYERS

Benchmark	QuCLEAR	Qiskit	Rustiq	PH	tket
LABS-(n10, 13)	296	896	337	690	521
LABS-(n15, 13)	1204	3632	1368	2640	2131
LABS-(n20, 13)	3262	8750	3841	6654	5594
MaxCut-(n15, r4, 13)	245	238	376	240	262
MaxCut-(n20, r12, 13)	506	718	605	720	799
MaxCut-(n20, e117, 13)	430	652	566	576	733

## IX. CONCLUSION

In this paper we propose QuCLEAR, a compilation framework for optimizing quantum circuits. We present two distinct techniques: Clifford Extraction and Clifford Absorption. We propose an efficient heuristic algorithm for synthesizing CNOT trees in quantum simulation circuits. Our approach leverages classical devices to efficiently simulate portions of the computations, leading to a reduced circuit size on quantum devices. Experimental results across various benchmarks demonstrate that QuCLEAR outperforms state-of-the-art methods in terms of both CNOT gate count and circuit depth.

## ACKNOWLEDGEMENTS

This material is based upon work supported by the U.S. Department of Energy, Office of Science, National Quantum Information Science Research Centers. This material is also based upon work supported by the DOE-SC Office of Advanced Scientific Computing Research AIDE-QC project under contract number DE-AC02-06CH11357.

The submitted manuscript has been created by UChicago Argonne, LLC, Operator of Argonne National Laboratory (“Argonne”). Argonne, a U.S. Department of Energy Office of Science laboratory, is operated under Contract No. DE-AC02-06CH11357. The U.S. Government retains for itself, and others acting on its behalf, a paid-up nonexclusive, irrevocable worldwide license in said article to reproduce, prepare derivative works, distribute copies to the public, and perform publicly and display publicly, by or on behalf of the Government. The Department of Energy will provide public access to these results of federally sponsored research in accordance with the DOE Public Access Plan. <http://energy.gov/downloads/doe-public-access-plan>.

## REFERENCES

- [1] J. Liu, L. Bello, and H. Zhou, “Relaxed peephole optimization: A novel compiler optimization for quantum circuits,” in *2021 IEEE/ACM International Symposium on Code Generation and Optimization (CGO)*. IEEE, 2021, pp. 301–314.
- [2] J. Liu, M. Bowman, P. Gokhale, S. Dangwal, J. Larson, F. T. Chong, and P. D. Hovland, “Qcontext: Context-aware decomposition for quantum gates,” in *2023 IEEE International Symposium on Circuits and Systems (ISCAS)*. IEEE, 2023, pp. 1–5.
- [3] Y. Jin, F. Hua, Y. Chen, A. Hayes, C. Zhang, and E. Z. Zhang, “Exploiting the regular structure of modern quantum architectures for compiling and optimizing programs with permutable operators,” in *Proceedings of the 28th ACM International Conference on Architectural Support for Programming Languages and Operating Systems, Volume 4*, 2023, pp. 108–124.
- [4] J. Zhou, Y. Liu, Y. Shi, A. Javadi-Abhari, and G. Li, “Bosehdral: Compiler optimization for bosonic quantum computing,” *arXiv preprint arXiv:2402.02279*, 2024.
- [5] M. Weiden, J. Kallor, J. Kubiawicz, E. Younis, and C. Iancu, “Wide quantum circuit optimization with topology aware synthesis,” in *2022 IEEE/ACM Third International Workshop on Quantum Computing Software (QCS)*. IEEE, 2022, pp. 1–11.
- [6] J. Liu, P. Li, and H. Zhou, “Not all swaps have the same cost: A case for optimization-aware qubit routing,” in *2022 IEEE International Symposium on High-Performance Computer Architecture (HPCA)*. IEEE, 2022, pp. 709–725.
- [7] J. Liu, E. Younis, M. Weiden, P. Hovland, J. Kubiawicz, and C. Iancu, “Tackling the qubit mapping problem with permutation-aware synthesis,” in *2023 IEEE International Conference on Quantum Computing and Engineering (QCE)*, vol. 1. IEEE, 2023, pp. 745–756.
- [8] C. Zhang, A. B. Hayes, L. Qiu, Y. Jin, Y. Chen, and E. Z. Zhang, “Time-optimal qubit mapping,” in *Proceedings of the 26th ACM International Conference on Architectural Support for Programming Languages and Operating Systems*, 2021, pp. 360–374.
- [9] C. Campbell, F. T. Chong, D. Dahl, P. Frederick, P. Goiporia, P. Gokhale, B. Hall, S. Issa, E. Jones, S. Lee *et al.*, “Superstaq: Deep optimization of quantum programs,” in *2023 IEEE International Conference on Quantum Computing and Engineering (QCE)*, vol. 1. IEEE, 2023, pp. 1020–1032.
- [10] R. Ayanzadeh, N. Alavisamani, P. Das, and M. Qureshi, “Frozenqubits: Boosting fidelity of qaoa by skipping hotspot nodes,” in *Proceedings of the 28th ACM International Conference on Architectural Support for Programming Languages and Operating Systems, Volume 2*, 2023, pp. 311–324.
- [11] A. Xu, A. Molavi, L. Pick, S. Tannu, and A. Albarghouthi, “Synthesizing quantum-circuit optimizers,” *Proceedings of the ACM on Programming Languages*, vol. 7, no. PLDI, pp. 835–859, 2023.
- [12] S. Dangwal, G. S. Ravi, L. M. Seifert, and F. T. Chong, “Clifford assisted optimal pass selection for quantum transpilation,” *arXiv preprint arXiv:2306.15020*, 2023.
- [13] H. Wang, P. Liu, D. B. Tan, Y. Liu, J. Gu, D. Z. Pan, J. Cong, U. A. Acar, and S. Han, “Atomique: A quantum compiler for reconfigurable neutral atom arrays,” in *2024 ACM/IEEE 51st Annual International Symposium on Computer Architecture (ISCA)*. IEEE, 2024, pp. 293–309.
- [14] A. Peruzzo, J. McClean, P. Shadbolt, M.-H. Yung, X.-Q. Zhou, P. J. Love, A. Aspuru-Guzik, and J. L. O’Brien, “A variational eigenvalue solver on a photonic quantum processor,” *Nature communications*, vol. 5, no. 1, p. 4213, 2014.
- [15] E. Farhi, J. Goldstone, and S. Gutmann, “A quantum approximate optimization algorithm,” *arXiv preprint arXiv:1411.4028*, 2014.
- [16] S. Lloyd, “Universal quantum simulators,” *Science*, vol. 273, no. 5278, pp. 1073–1078, 1996.
- [17] H. F. Trotter, “On the product of semi-groups of operators,” *Proceedings of the American Mathematical Society*, vol. 10, no. 4, pp. 545–551, 1959.
- [18] D. Poulin, M. B. Hastings, D. Wecker, N. Wiebe, A. C. Doherty, and M. Troyer, “The trotter step size required for accurate quantum simulation of quantum chemistry,” *Quantum Information & Computation*, vol. 15, no. 5-6, pp. 361–384, 2015.
- [19] S. Ræisi, N. Wiebe, and B. C. Sanders, “Quantum-circuit design for efficient simulations of many-body quantum dynamics,” *New Journal of Physics*, vol. 14, no. 10, p. 103017, 2012.
- [20] Z. Jiang, K. J. Sung, K. Kechedzhi, V. N. Smelyanskiy, and S. Boixo, “Quantum algorithms to simulate many-body physics of correlated fermions,” *Physical Review Applied*, vol. 9, no. 4, p. 044036, 2018.
- [21] G. G. Guerreschi and A. Y. Matsuura, “Qaoa for max-cut requires hundreds of qubits for quantum speed-up,” *Scientific reports*, vol. 9, no. 1, p. 6903, 2019.
- [22] H. R. Grimsley, D. Claudino, S. E. Economou, E. Barnes, and N. J. Mayhall, “Is the trotterized uccsd ansatz chemically well-defined?” *Journal of chemical theory and computation*, vol. 16, no. 1, pp. 1–6, 2019.
- [23] S. Khairy, R. Shayduln, L. Cincio, Y. Alexeev, and P. Balaprakash, “Learning to optimize variational quantum circuits to solve combinatorial problems,” in *Proceedings of the AAAI conference on artificial intelligence*, vol. 34, no. 03, 2020, pp. 2367–2375.
- [24] Y. Kim, A. Eddins, S. Anand, K. X. Wei, E. Van Den Berg, S. Rosenblatt, H. Nayfeh, Y. Wu, M. Zaletel, K. Temme *et al.*, “Evidence for the utility of quantum computing before fault tolerance,” *Nature*, vol. 618, no. 7965, pp. 500–505, 2023.

- [25] G. Li, A. Wu, Y. Shi, A. Javadi-Abhari, Y. Ding, and Y. Xie, "Paulihedral: a generalized block-wise compiler optimization framework for quantum simulation kernels," in *Proceedings of the 27th ACM International Conference on Architectural Support for Programming Languages and Operating Systems*, 2022, pp. 554–569.
- [26] Y. Jin, Z. Li, F. Hua, Y. Chen, H. Chen, Y. Huang, and E. Z. Zhang, "Tetris: A compilation framework for vqe applications," *arXiv preprint arXiv:2309.01905*, 2023.
- [27] A. Cowtan, S. Dilkes, R. Duncan, W. Simmons, and S. Sivarajah, "Phase gadget synthesis for shallow circuits," *arXiv preprint arXiv:1906.01734*, 2019.
- [28] A. Cowtan, W. Simmons, and R. Duncan, "A generic compilation strategy for the unitary coupled cluster ansatz," *arXiv preprint arXiv:2007.10515*, 2020.
- [29] E. Van Den Berg and K. Temme, "Circuit optimization of hamiltonian simulation by simultaneous diagonalization of pauli clusters," *Quantum*, vol. 4, p. 322, 2020.
- [30] T. G. de Brugière and S. Martiel, "Faster and shorter synthesis of hamiltonian simulation circuits," *arXiv preprint arXiv:2404.03280*, 2024.
- [31] Y. Cao, J. Romero, J. P. Olson, M. Degroote, P. D. Johnson, M. Kieferová, I. D. Kivlichan, T. Menke, B. Peropadre, N. P. Sawaya *et al.*, "Quantum chemistry in the age of quantum computing," *Chemical reviews*, vol. 119, no. 19, pp. 10856–10915, 2019.
- [32] J. Romero, R. Babbush, J. R. McClean, C. Hempel, P. J. Love, and A. Aspuru-Guzik, "Strategies for quantum computing molecular energies using the unitary coupled cluster ansatz," *Quantum Science and Technology*, vol. 4, no. 1, p. 014008, 2018.
- [33] M. A. Nielsen and I. L. Chuang, *Quantum computation and quantum information*. Cambridge university press, 2010.
- [34] D. Gottesman, "The heisenberg representation of quantum computers," *arXiv preprint quant-ph/9807006*, 1998.
- [35] C. Gidney, "Stim: a fast stabilizer circuit simulator," *Quantum*, vol. 5, p. 497, 2021.
- [36] G. Li, Y. Shi, and A. Javadi-Abhari, "Software-hardware co-optimization for computational chemistry on superconducting quantum processors," in *2021 ACM/IEEE 48th Annual International Symposium on Computer Architecture (ISCA)*. IEEE, 2021, pp. 832–845.
- [37] K. Gui, T. Tomesh, P. Gokhale, Y. Shi, F. T. Chong, M. Martonosi, and M. Suchara, "Term grouping and travelling salesperson for digital quantum simulation," *arXiv preprint arXiv:2001.05983*, 2020.
- [38] J. Paykin, A. T. Schmitz, M. Ibrahim, X.-C. Wu, and A. Y. Matsuura, "Pcoast: a pauli-based quantum circuit optimization framework," in *2023 IEEE International Conference on Quantum Computing and Engineering (QCE)*, vol. 1. IEEE, 2023, pp. 715–726.
- [39] A. T. Schmitz, N. P. Sawaya, S. Johri, and A. Matsuura, "Graph optimization perspective for low-depth trotter-suzuki decomposition," *Physical Review A*, vol. 109, no. 4, p. 042418, 2024.
- [40] S. Sivarajah, S. Dilkes, A. Cowtan, W. Simmons, A. Edgington, and R. Duncan, "t—ket<sub>q</sub>: a retargetable compiler for nisq devices," *Quantum Science and Technology*, vol. 6, no. 1, p. 014003, 2020.
- [41] M. Amy, P. Azimzadeh, and M. Mosca, "On the controlled-not complexity of controlled-not-phase circuits," *Quantum Science and Technology*, vol. 4, no. 1, p. 015002, 2018.
- [42] X.-C. Wu, S. P. Premaratne, and K. Rasch, "A comprehensive introduction to the intel quantum sdk," in *Proceedings of the 2023 Introduction on Hybrid Quantum-Classical Programming Using C++ Quantum Extension*, 2023, pp. 1–2.
- [43] S. Aaronson and D. Gottesman, "Improved simulation of stabilizer circuits," *Physical Review A—Atomic, Molecular, and Optical Physics*, vol. 70, no. 5, p. 052328, 2004.
- [44] D. Wecker, B. Bauer, B. K. Clark, M. B. Hastings, and M. Troyer, "Gate-count estimates for performing quantum chemistry on small quantum computers," *Physical Review A*, vol. 90, no. 2, p. 022305, 2014.
- [45] M. B. Hastings, D. Wecker, B. Bauer, and M. Troyer, "Improving quantum algorithms for quantum chemistry," *arXiv preprint arXiv:1403.1539*, 2014.
- [46] P. Gokhale, O. Angiuli, Y. Ding, K. Gui, T. Tomesh, M. Suchara, M. Martonosi, and F. T. Chong, " $\mathcal{O}(n^3)$  measurement cost for variational quantum eigensolver on molecular hamiltonians," *IEEE Transactions on Quantum Engineering*, vol. 1, pp. 1–24, 2020.
- [47] K. Nakaji, S. Endo, Y. Matsuzaki, and H. Hakoshima, "Measurement optimization of variational quantum simulation by classical shadow and derandomization," *Quantum*, vol. 7, p. 995, 2023.
- [48] A. Lucas, "Ising formulations of many np problems," *Frontiers in physics*, vol. 2, p. 5, 2014.
- [49] A. Boehmer, "Binary pulse compression codes," *IEEE Transactions on Information Theory*, vol. 13, no. 2, pp. 156–167, 1967.
- [50] R. Shaydulin, C. Li, S. Chakrabarti, M. DeCross, D. Herman, N. Kumar, J. Larson, D. Lykov, P. Minssen, Y. Sun *et al.*, "Evidence of scaling advantage for the quantum approximate optimization algorithm on a classically intractable problem," *Science Advances*, vol. 10, no. 22, p. eadm6761, 2024.
- [51] P. K. Barkoutsos, J. F. Gonthier, I. Sokolov, N. Moll, G. Salis, A. Fuhrer, M. Ganzhorn, D. J. Egger, M. Troyer, A. Mezzacapo *et al.*, "Quantum algorithms for electronic structure calculations: Particle-hole hamiltonian and optimized wave-function expansions," *Physical Review A*, vol. 98, no. 2, p. 022322, 2018.
- [52] I. G. Ryabinkin, T.-C. Yen, S. N. Genin, and A. F. Izmaylov, "Qubit coupled cluster method: a systematic approach to quantum chemistry on a quantum computer," *Journal of Chemical Theory and Computation*, vol. 14, no. 12, pp. 6317–6326, 2018.
- [53] S. E. Smart, J.-N. Boyn, and D. A. Mazziotti, "Resolving correlated states of benzyne with an error-mitigated contracted quantum eigensolver," *Physical Review A*, vol. 105, no. 2, p. 022405, 2022.
- [54] A. Javadi-Abhari, M. Treinish, K. Krsulich, C. J. Wood, J. Lishman, J. Gacon, S. Martiel, P. D. Nation, L. S. Bishop, A. W. Cross, B. R. Johnson, and J. M. Gambetta, "Quantum computing with Qiskit," 2024.
- [55] S. Klabnik and C. Nichols, *The Rust programming language*. No Starch Press, 2023.